Journal of Medicinal Chemistry

Article

The Application of 3D-QSAR Studies for Novel Cannabinoid Ligands Substituted at the C1‘ Position of the Alkyl Side Chain on the Structural Requirements for Binding to Cannabinoid Receptors CB1 and CB2

Serdar Durdagi, Agnes Kapou, Therapia Kourouli, Thanos Andreou, Spyros P. Nikas, Victoria R. Nahmias, Demetris P. Papahatjis, Manthos G. Papadopoulos, and Thomas Mavromoustakos

J. Med. Chem., **2007**, 50 (12), 2875-2885 • DOI: 10.1021/jm0610705

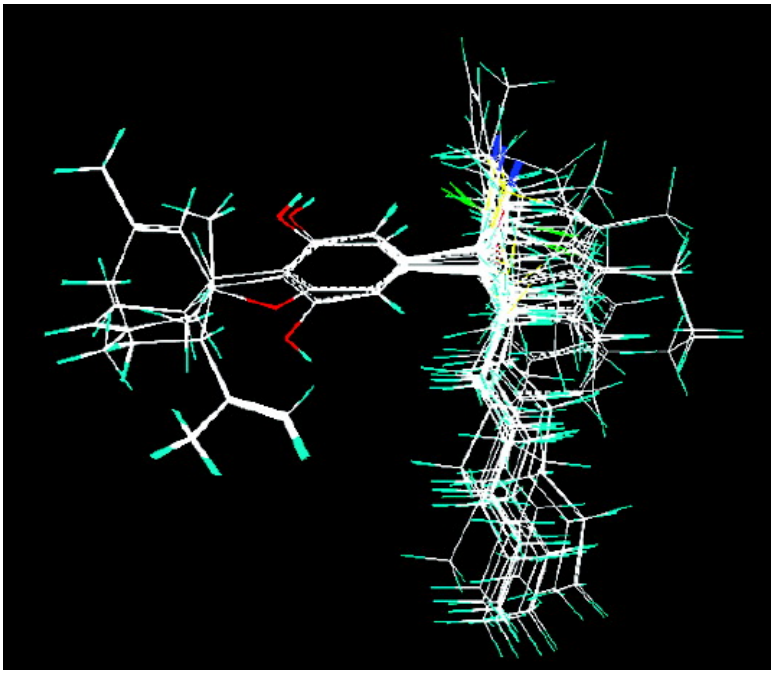

More About This Article

Additional resources and features associated with this article are available within the HTML version:

- Supporting Information
- Links to the 6 articles that cite this article, as of the time of this article download
- Access to high resolution figures
- Links to articles and content related to this article
- Copyright permission to reproduce figures and/or text from this article

Journal of Medicinal Chemistry is published by the American Chemical Society. 1155 Sixteenth Street N.W., Washington, DC 20036

The Application of 3D-QSAR Studies for Novel Cannabinoid Ligands Substituted at the C1′ Position of the Alkyl Side Chain on the Structural Requirements for Binding to Cannabinoid Receptors CB1 and CB2

Serdar Durdagi,[†,‡] Agnes Kapou,[†] Therapia Kourouli,[†] Thanos Andreou,[†] Spyros P. Nikas,[§] Victoria R. Nahmias,[†] Demetris P. Papahatjis,[†] Manthos G. Papadopoulos,[†] and Thomas Mavromoustakos*[,†]

Institute of Organic and Pharmaceutical Chemistry, The National Hellenic Research Foundation, 48 Vas. Constantinou Avenue, 11635 Athens, Greece, Department of Biology, Chemistry and Pharmacy, Freie Universität Berlin, Takustr. 3, 14195 Berlin, Germany, and Center for Drug Discovery, Northeastern University, 116 Mugar Hall, 360 Huntington Avenue, Boston, Massachusetts 02115

Received September 11, 2006

A set of 30 novel Δ^8-tetrahydrocannabinol and cannabidiol analogues were subjected to three-dimensional quantitative structure−activity relationship studies using the comparative molecular field analysis (CoMFA) and comparative molecular similarity indices analysis (CoMSIA) approaches. Using a combination of molecular modeling techniques and NMR spectroscopy, the putative bioactive conformation of the most potent cannabinoid (CB) ligand in the training set was determined. This conformer was used as the template and CB1 and CB2 pharmacophore models were developed. These models were fitted with experimental binding data and gave high correlation coefficients. Contour maps of the CB1 and CB2 models of CoMFA and CoMSIA approaches show that steric effects dominantly determine the binding affinities. The CoMFA and CoMSIA analyses based on the binding affinity data of CB ligands at the CB1 and CB2 receptors allowed us to deduce the possible optimal binding positions. This information can be used for the design of new CB analogues with enhanced activity and other tailored properties.

Introduction

Cannabis sativa L. is one of the oldest known medicinal plants and has been extensively used with respect to its psychotropic and pharmacological effects. Δ^9-Tetrahydrocannabinol (Δ^9-THC; Figure 1a) is the primary psychoactive constituent of cannabis and it was identified by Gaoni and Mechoulam in 1964.[1]

The pharmacological activity of cannabinoids (CBs[a]) is mediated by two CB receptors: CB1[2−5] and CB2.[6] Both CB1 and CB2 receptors belong to the Class A, membrane-bound rhodopsin-like family of G-protein coupled receptors, possessing seven characteristic transmembrane domains.[7−9] The CB1 receptor is abundant especially in the central nervous system[10,11] and peripheral tissues[12] and is assumed to be involved in the regulation of cognition, memory, motor activity, and the inhibition of transmitter release through its coupling to Ca^{2+} and K^+ channels. The CB2 receptor, on the other hand, is exclusively present in the tonsils and cells of the immune system,[13,14] such as B lymphocytes and macrophages. It is also found in the marginal zone of the spleen. The CB2 receptor is assumed to participate in the regulation of immune responses and inflammatory reactions. Pharmacological studies have shown that CBs possess many potential therapeutic applications including against cancer, AIDS, stroke, pain, obesity, cachexia, and neuronal disorders such as multiple sclerosis, Huntington's chorea, and Parkinson's disease, as well as reduction of blood ocular pressure in glaucomic patients.[15−23]

CBs can be classified mainly into three categories: natural (herbal) or classical CBs, endogenous CBs, and synthetic CBs. Natural CBs occur in the cannabis plant. Tetrahydrocannabinol (THC), cannabidiol (CBD), and cannabinol are examples of natural CBs. Endogenous CBs are produced in the bodies of human and animals. An endogenous CB ligand was isolated from porcine brain by Mechoulam et al. in 1992[24] and was identified as arachidonylethanolamide (anandamide). It binds to the CB1 and CB2 receptors with modest (K_i = 61 nM) and with low (K_i = 1930 nM) affinities, respectively.[24] It behaves as a partial agonist in the biochemical and pharmacological tests used to characterize CB activity.[15,25] 2-Arachidonyl glycerol (2-AG) is the second identified endogenous CB and was isolated from brain and intestinal tissues by the Sugiura and Mechoulam groups.[26,27] It was found to bind weakly to both CB1 (K_i = 472 nM) and CB2 (K_i = 1400 nM) receptors. In part, because of its nonsignaling role as an intermediate in several lipid metabolic pathways, 2-AG is far more abundant than anandamide.[7,28,29] Prior to the discovery of CB receptors, a number of independent research laboratories and pharmaceutical industries developed a large number of synthetic CB ligands as pharmacological and biochemical probes for studying CB biology and also prototypes for developing new medications. HU-210, CP55,940, and nabilone are examples of such synthetic CB analogues.[30] The discovery of endogenous ligands prompted further studies aimed at the elucidation of the chemical and pharmacological behavior of the CB1 and CB2 receptors and cannabinomimetic ligands. These studies pointed out that, in addition to classical CBs, other structurally different molecules may interact with the same receptors, inducing analogous responses.[16,31] Both classical and nonclassical CBs possess four pharmacophores within the CB prototype: a phenolic hydroxyl, a lipophilic side chain, a northern aliphatic hydroxyl, and a southern aliphatic hydroxyl. The early structure−activity relationship (SAR) studies have been reviewed comprehensively by Thakur et al.,[15] by Khanolkar et al.,[17] by Razdan,[32] and by Makriyannis and Rapaka.[33] Earlier literature reports[7,15,32−34]

* To whom correspondence should be addressed. Tel.: +30-210-72-73-869. Fax: +30-210-72-73-872. E-mail: tmavro@eie.gr.
† The National Hellenic Research Foundation.
‡ Freie Universität Berlin.
§ Northeastern University.

[a] Abbreviations: CB, cannabinoid; CBD, cannabidiol; THC, tetrahydrocannabinol; 2-AG, 2-arachidonyl glycerol; r^2_{cv}, cross-validated r^2.

10.1021/jm0610705 CCC: $37.00
Published on Web 05/24/2007

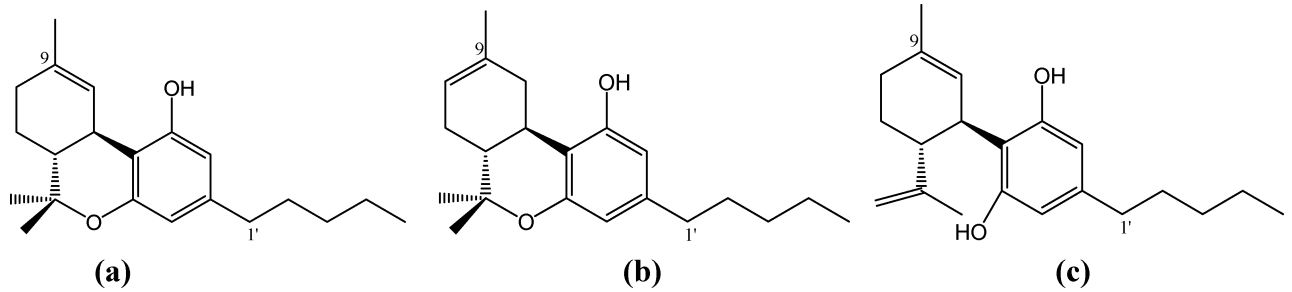

Figure 1. Chemical structures of (a) Δ^9-THC, (b) Δ^8-THC, (c) CBD.

showed that the lipophilic alkyl side chain plays a crucial role in determining cannabimimetic activity and selectivity toward CB receptors, as well as pharmacological potency. The alkyl side chain fits into a hydrophobic pocket such that the chain is oriented nearly perpendicular to the aromatic ring A.[7,35−38] Analogues with alkyl side chains of less than five carbons have limited affinity for the CB1 receptor.[15,17] Extension of the five-carbon chain by adding one or two carbons improves binding, while further extension is detrimental to binding due to steric hindrance. Structural variations within this pharmacophore can result in analogues varying by up to 3 orders of magnitude in binding affinity for the CB receptor and in pharmacological potency. The structural modifications of the side chain produce high affinity ligands with either antagonist, partial agonist, or full agonist effects.[7]

To improve the medicinal properties and eliminate or reduce untoward effects, medicinal chemists are designing, synthesizing, and testing additional CB1 and CB2 ligands. The main effort of our laboratory is to explore the pharmacophoric requirements of the alkyl side chain within the classical Δ^8-THC (Figure 1b) and CBD (Figure 1c) templates. Δ^8-THC has a very similar pharmacologic profile as Δ^9-THC, however, it is chemically more stable. Several cannabinergic ligands possessing high affinities for both of the CB receptors have been developed recently. One of the most successful compounds that resulted from this work was the C1′-dithiolane analogue; (−)-2-(6a,7,10,10a-tetrahydro-6,6,9-trimethyl-1-hydroxy-6*H*-dibenzo[b,d]pyranyl)-2-hexyl-1,3-dithiolane (**12** in Table 1), exerting binding affinity (K_i) values of 0.32 and 0.52 nM for the CB1 and CB2 receptors, respectively.[34]

Hitherto, no direct observation of a CB ligand bound to a CB receptor using X-ray crystallography has been reported.[39] Therefore, active sites of these receptors have been postulated from many approaches, such as receptor binding analyses of a variety of CB derivatives using wild type and mutated receptor systems, molecular modeling analysis, and three-dimensional quantitative SAR (3D-QSAR) studies.[39−45] Results of studies on 3D-QSAR models of novel CBs using comparative molecular field analysis (CoMFA), developed by R. Cramer et al.,[46] and comparative molecular similarity indices analysis (CoMSIA), developed by Klebe et al.,[47] have been reported. These techniques have been successfully used previously in 3D-QSAR studies of CBs and other ligands.[21,39,43,48−54] The present study uses 3D-QSAR CoMFA and CoMSIA analyses on novel CB analogues (Table 1) with a wide variation of biological activity (1200- and 4000-fold variances in bioactivity for the CB2 and CB1 receptors, respectively). These compounds are characterized by subtle structural variations and a wide range of biological activities which constitute an ideal base for 3D-QSAR studies.

The aim of applying 3D-QSAR CoMFA and CoMSIA studies is to derive indirect binding information from the correlation between the biological activity of a training set of molecules and their 3D structure. The importance of steric and electrostatic characteristics are revealed by aligning structurally similar analogues using pharmacophoric features as structural superimposition guides. CoMFA calculates steric and electrostatic properties in the space surrounding each of the aligned molecules in a data set according to Lennard−Jones and Coulomb potentials, respectively. CoMSIA calculates similarity indices around the molecules, with the similarity expressed in terms of different physicochemical properties, such as steric occupancy, partial atomic charges, local hydrophobicity, and hydrogen bond donor and acceptor properties.[48,55] The use of CoMFA and CoMSIA approaches together provide better ability of visualization and interpretation of the obtained correlations in terms of field contributions. Using a combination of molecular modeling techniques and NMR spectroscopy, the putative bioactive conformation of the most potent ligand in the training set was determined and was used as a template and CB1 and CB2 pharmacophore models were developed.[38] Each generated 3D-QSAR model allowed us to anticipate the predicted binding affinity values. To determine the linear correlation coefficients between actual versus calculated binding affinities, partial least-square (PLS) statistical analyses of the data were used. CoMFA and CoMSIA contour plots are used to explain different structural requirements for CB binding to the CB1 and CB2 receptors. Contour results can be used as pilot models for testing the designed novel analogues before their synthesis.

Results

For the CoMFA and CoMSIA analyses of CB ligands binding to the CB1 and CB2 receptors, structural alignment of all compounds in the training set (Table 1) was performed. Table 1 lists all structures used in the training set and the experimental binding affinities (K_i) with the CB1 and CB2 receptors.[34,56−59] Among the synthesized analogues, **12** (Figure 2) was selected as a template, because (i) there is adequate information supporting the proposed conformation of **12**, derived by the combined application of NMR and molecular modeling studies[38] and (ii) it has the highest binding affinity to the CB1 receptor ($K_i = 0.32$ nM) and second highest binding affinity to the CB2 receptor ($K_i = 0.52$ nM) in the training set.[34] The high binding affinity of **12** can be attributed to two causes. First, its increased hydrophobicity of the side chain due to the benzylic substitution may favor interactions with a corresponding hydrophobic subsite of the receptors, and second, the side chain pharmacophore is conformationally more defined than the Δ^8-THC prototype CB.[38]

The lowest energy conformer of **12** and other Δ^8-THC derivatives have been obtained and reported using a combination of NMR spectroscopy and molecular modeling techniques.[38,56] In addition, the conformation of the flexible l′,l′-dimethylheptyl side chain was analyzed using a combination of theoretical and NMR studies for classical (−)-9-nor-9β-hydroxy(dimethylheptyl)-hexahydrocannabinol and nonclassical CBs CP47,497, CP55,244, and CP55,940 by Xie et al.[35,60,61] The obtained results showed that the C3-alkyl side chain is almost perpendicular to

Table 1. Molecular Structures and Binding Affinity K_i Values of CB Analogues Used as the Training Set to Construct CoMFA and CoMSIA Models[34,56−59]

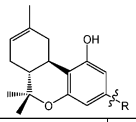
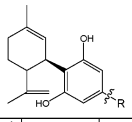

Compound No.	R	K_i for CB1 (nM)	K_i for CB2 (nM)	Compound No.	Ki for CB1 (nM)	Ki for CB2 (nM)
1		95.49	71.81	**2**	638.1	374.4
3		119.0	51.70			
4	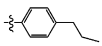	57.77	107.80			
5		11.73	9.39	**6**	753.5	221.6
7		27.90	25.20	**8**	255.0	105.0
9		8.26	3.86	**10**	319.0	110.7
11		168.0	103.0			
12	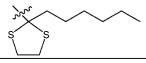	0.32	0.52	**13**	136.0	50.40
14	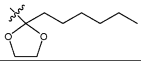	0.52	0.22			
15	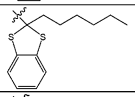	56.90	257.0			
16	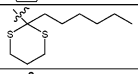	1.80	3.60			
17	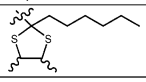	32.30	19.70			
18	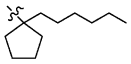	0.45	1.92			
19	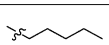	47.60	39.30	**20**	1265.0	230.0
21	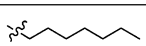	22.00	-			
22	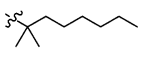	0.83	0.49			
23	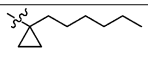	0.44	0.86	**24**	58.68	99.23
25	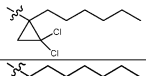	1.27	0.29	**26**	666.4	32.87
27	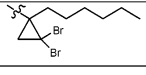	0.71	1.03	**28**	189.0	63.30
29	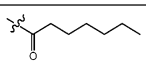	21.70	83.70			
30	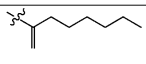	2.17	3.30			

the plane of ring A. Molecular docking models of CP47,497, CP55,244, and CP55,940 have also been examined by Shim et al.,[62] and the authors reported that the C3-alkyl side chain is oriented perpendicular to the ring A.

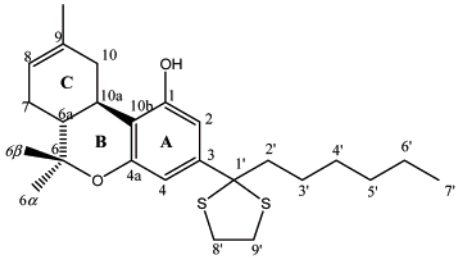

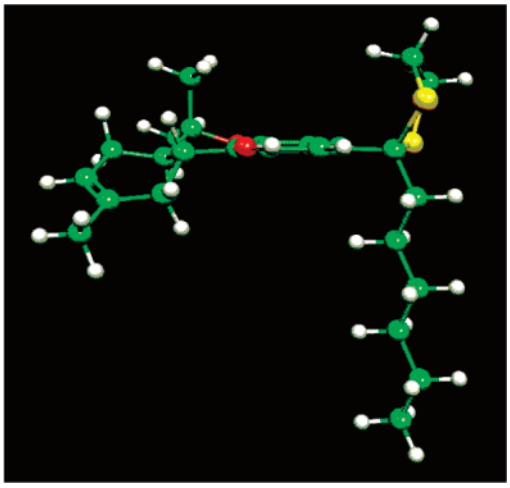

Figure 2. Molecular structure of template compound **12** (on the top) and its lowest energy conformer (on the bottom).

Several researchers have argued that conformation, orientation, and location of the drug molecule in the membrane play a crucial role in determining the ability of the drug to interact favorably with its site of action on the receptor.[63,64] Biophysical studies by Makriyannis and co-workers have provided detailed information on the topography, stereochemistry, and dynamic features of the CB−membrane interactions using neutron diffraction, solid state ^{2}H NMR, small-angle X-ray spectroscopy, and differential scanning calorimetry.[63] In these studies, THC assumes an "awkward" orientation in the bilayer with the long axis of its tricyclic system perpendicular to the bilayer chains, while its aliphatic side chain orients parallel to the chains of the membrane phospholipids.

The existing experimental evidence combined with performed ab initio B3LYP/6-31G*[65,66] level of quantum mechanics (QM) calculations show undoubtedly that the lowest energy conformation of **12** (Figure 2) must be used as a suitable template for superimposition studies in the 3D-QSAR CoMFA and CoMSIA methods.

Several variations in the alignment schemes by superimposing the similar pharmacophoric features are considered. C_1, C_2, C_3, C_4, C_{4a}, C_{6a}, C_7, C_{10}, C_{10a}, and C_{10b} and the oxygen atoms in the template ligand **12** are selected for the structural superimposition processes. The alignment of the molecules was based on atom-by-atom superimposition of selected atoms, which is common in all compounds. The criteria applied for the selection were (i) overlap of the putative biologically relevant pharmacophore groups (with minimum RMS) and (ii) form of statistically significant 3D-QSAR CoMFA and CoMSIA models. Figure 3 illustrates the superimposition of CB analogues used as the training set to construct CoMFA and CoMSIA models.

To build 3D-QSAR CoMFA and CoMSIA models for the binding affinity at the CB1 and CB2 receptors, a set of 30 CB analogues for the CB1 receptor and 29 CB analogues for the CB2 receptor were subjected to the cross-validated PLS analyses.

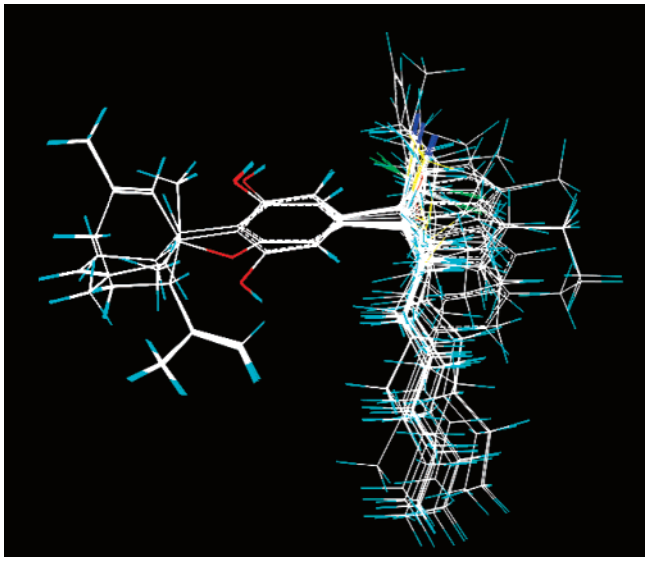

Figure 3. Structural alignments of the compounds in the training set for constructing 3D-QSAR CoMFA and CoMSIA models at the CB1 and CB2 receptors.

Table 2. Cross-Validated Analyses for the CB1 and CB2 Receptors Using the CoMFA Models, Based on the **12** as Template

model	template compound	number of compounds in the training set	r^2_{cv}	number of optimal components
CB1	**12** in Table 1	30	0.784	6
CB2	**12** in Table 1	29	0.572	6

(i) CoMFA Results. Table 2 shows the cross-validated r^2 (r^2_{cv}) values using CoMFA analyses at CB receptors. The CoMFA study, based on the selected lowest energy conformer of template ligand **12**, gave r^2_{cv} values of 0.784 and 0.572 for CB1 and CB2 receptors, respectively. The noncross-validated PLS analysis yielded an r^2 of 0.981 and 0.972, and the estimated standard errors were 0.173 and 0.187 for CB1 and CB2 receptors, respectively (Table 3). Therefore, the CoMFA-generated 3D-QSAR models for the binding affinities of CB analogues to CB1 and CB2 receptors have a very good cross-validated correlation. Figure 4 shows the relationship between the CoMFA-predicted and experimental pK_i values of the noncross-validated analyses for CB1 and CB2 receptors. Linearity of the plots show very good correlations for CoMFA models developed in the study for the binding affinities of CBs at the CB1 and CB2 receptor sites.

CoMFA Contour Maps. The contour maps are used to create a "negative" matrix in the place of the unknown active site, and variations of the used ligands can be generated as long as they fit better into the "imaginary" active site. Figure 5a,b shows the steric-electrostatic contour maps of the CoMFA models for CB1 and CB2 receptors, respectively. The individual contributions from the steric and electrostatic favored and disfavored levels are fixed at 80% and 20%, respectively. The CoMFA contours of the steric maps are shown in yellow and green colors and those of the electrostatic contour maps are shown in red and blue colors. Greater values of "bioactive measurement" are collected, with more bulk near the green-colored contours; less bulk near the yellow-colored contours; more positive charge near the blue-colored contours; and more negative charge near the red-colored contours.

(ii) CoMSIA Results. The CoMSIA study, based on the selected lowest energy conformer of template ligand **12**, gave

Table 3. Summary of Experimental (Observed) and CoMFA-Predicted pK_i Results for the Binding Affinity at the CB1 and CB2 Receptors

	CB1 CoMFA model	CB2 CoMFA model
r^2	0.981	0.972
standard error of estimate	0.173	0.187
probability of r^2	0.000	0.000
F	197.531	127.260
relative contributions of steric/electrostatic fields	0.640:0.360	0.632:0.368
$r^2_{bootsrapping}$	0.990	0.989
standard error of estimate$_{bootstapping}$	0.121	0.117

	CB1 CoMFA model		CB2 CoMFA model	
cmpd	pK_i (observed)	pK_i (predicted)	pK_i (observed)	pK_i (predicted)
1	7.02	7.16	7.14	7.25
2	6.20	6.18	6.43	6.50
3	6.92	7.09	7.29	7.19
4	7.24	7.13	6.97	7.13
5	7.93	7.86	8.03	7.98
6	6.12	6.20	6.65	6.64
7	7.55	7.69	7.60	7.87
8	6.59	6.63	6.98	7.03
9	8.08	8.09	8.41	8.27
10	6.50	6.56	6.96	7.03
11	6.77	6.66	6.99	6.95
12	9.49	9.34	9.28	8.96
13	6.87	6.89	7.30	7.39
14	9.28	9.40	9.66	9.68
15	7.24	7.17	6.59	6.62
16	8.74	8.74	8.44	8.44
17	7.49	7.61	7.71	7.68
18	9.35	9.50	8.72	9.05
19	7.32	7.33	7.41	7.51
20	5.90	5.80	6.64	6.43
21	7.66	7.73	-	-
22	9.08	8.99	9.31	9.04
23	9.36	9.13	9.07	9.12
24	7.23	6.88	7.00	7.16
25	8.90	9.19	9.54	9.35
26	6.18	6.53	7.48	7.19
27	9.15	9.11	8.99	9.29
28	6.72	6.58	7.20	7.26
29	7.66	7.52	7.08	6.93
30	8.66	8.54	8.48	8.39

r^2_{cv} values of 0.746 and 0.625 for the CB1 and CB2 receptors, respectively (Table 4). The noncross-validated PLS analysis yielded an r^2 of 0.944 and 0.912, and the estimated standard errors were 0.296 and 0.324 for CB1 and CB2 receptors, respectively (Table 5). Figure 6 shows the relationship between the CoMSIA predicted and the CoMSIA experimental pK_i values for the noncross-validated analyses of CB1 and CB2 receptors.

CoMSIA Contour Maps. Figure 7a,b shows the steric-electrostatic contour maps of the CoMSIA models for the CB1 and CB2 receptors, respectively. The individual contributions from the steric and electrostatic favored and disfavored levels are fixed at 80% and 20%, respectively. The CoMSIA contours of the steric maps are shown in yellow and green colors, and those of the electrostatic contour maps are shown in red and blue colors. Greater values of "bioactive measurement" are collected with more bulk near the green-colored contours; less bulk near the yellow-colored contours; more positive charge near the blue-colored contours; and more negative charge near the red-colored contours.

Because the CB analogues used in the training set differ mainly in the C1′ position and the tricyclic part of Δ^8-THC or

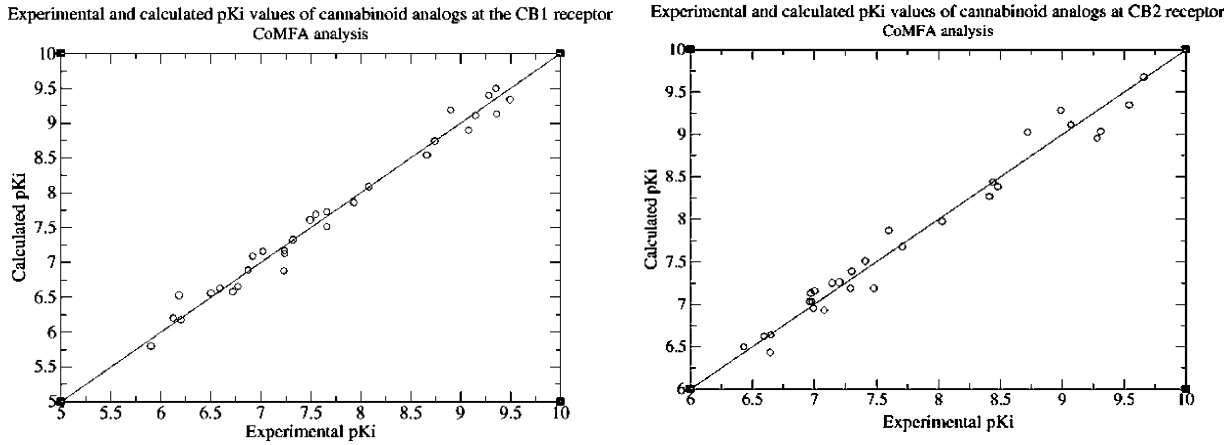

Figure 4. Plots of corresponding CoMFA-predicted and experimental values of binding affinity (given as pK_i) of CB analogues in the training set at the CB1 (on the left) and CB2 (on the right) receptors, respectively.

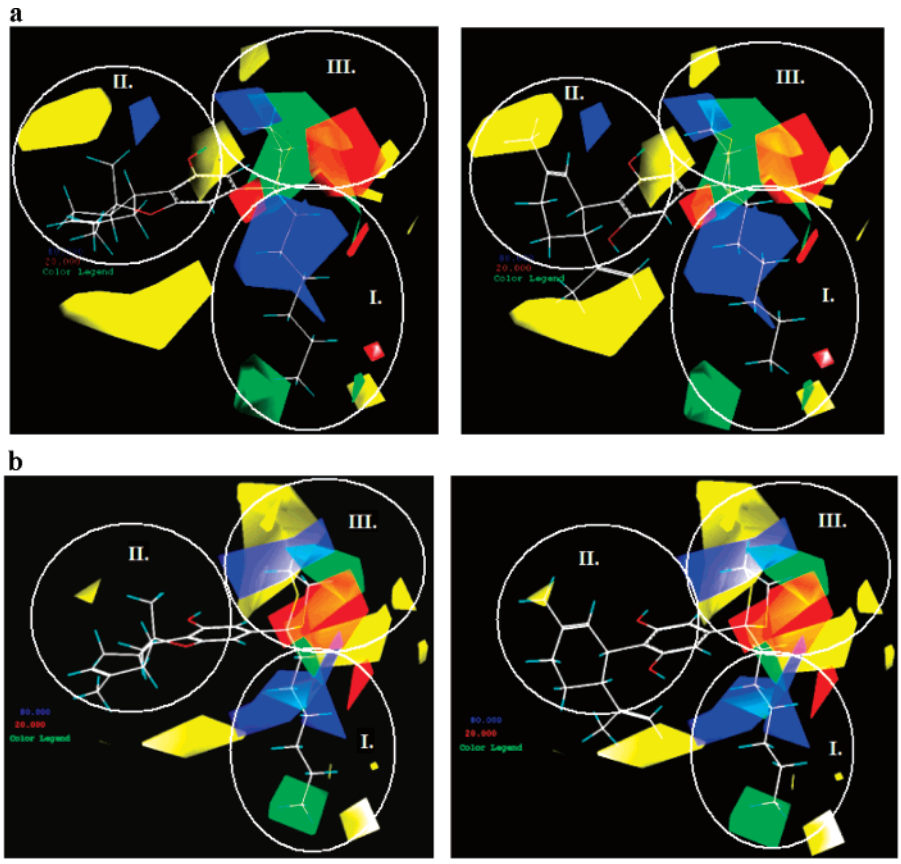

Figure 5. (a) CoMFA contour maps of template compound **12** (on the left) and its respective CBD analogue **13** (on the right) for the CB1 model. Sterically favored areas are shown in green (contribution level of 80%). Sterically unfavored areas are shown in yellow (contribution level of 20%). Positive potential favored areas are shown in blue (contribution level of 80%). Positive potential unfavored areas are shown in red (contribution level of 20%). (Regions I, II, and III show contour maps around the alkyl side chain, the tricyclic part, and the α-face of C1′ of the ligand, respectively.) (b) CoMFA contour maps of template compound **12** (on the left) and its respective CBD analog **13** (on the right) for the CB2 model. Sterically favored areas are shown in green (contribution level of 80%). Sterically unfavored areas are shown in yellow (contribution level of 20%). Positive potential favored areas are shown in blue (contribution level of 80%). Positive potential unfavored areas are shown in red (contribution level of 20%). (Regions I, II, and III show contour maps around alkyl side chain, tricyclic part and α-face of C1′ of the ligand, respectively.)

the CBD skeleton, the contour plots place more emphasis to these regions. The main topographical requirements for the CB1 and CB2 receptors resulting from the CoMFA and CoMSIA approaches are summarized and presented in the Supporting Information.

Table 4. Cross-validated Analyses for the CB1 and CB2 Receptors Using the CoMSIA Models, Based on the **12** as Template

model	template compound	number of compounds in training set	r^2_{cv}	number of optimal components
CB1	**12** in Table 1	30	0.746	6
CB2	**12** in Table 1	29	0.625	5

Discussion

The main differences between the 3D-QSAR CoMFA and the 3D-QSAR CoMSIA approaches concern the type of distance dependent function used and the form of the defined probe atom. In CoMFA, the probe atom is a sp^3 carbon with a +1.0

Table 5. Summary of Experimental (Observed) and CoMSIA-Predicted pK_i Results for the Binding Affinity at the CB1 and CB2 Receptors

	CB1 CoMSIA model	CB2 CoMSIA model
r^2	0.944	0.912
standard error of estimate	0.296	0.324
probability of r^2	0.000	0.000
F	65.031	47.855
relative contributions of steric/electrostatic fields	0.890:0.110	0.918:0.082
$r^2_{\text{bootsrapping}}$	0.971	0.972
standard error of estimate$_{\text{bootstapping}}$	0.206	0.181

	CB1 CoMSIA model		CB2 CoMSIA model	
cmpd	pK_i (observed)	pK_i (predicted)	pK_i (observed)	pK_i (predicted)
1	7.02	7.19	7.14	7.31
2	6.20	6.12	6.43	6.43
3	6.92	7.03	7.29	7.19
4	7.24	6.98	6.97	7.15
5	7.93	7.54	8.03	7.74
6	6.12	6.40	6.65	6.75
7	7.55	7.63	7.60	7.97
8	6.59	6.51	6.98	7.01
9	8.08	7.83	8.41	8.18
10	6.50	6.51	6.96	7.08
11	6.77	6.91	6.99	7.04
12	9.49	9.00	9.28	8.68
13	6.87	6.89	7.30	6.99
14	9.28	9.20	9.66	9.18
15	7.24	7.15	6.59	6.99
16	8.74	8.45	8.44	8.43
17	7.49	8.03	7.71	8.10
18	9.35	9.82	8.72	9.32
19	7.32	7.33	7.41	7.46
20	5.90	5.98	6.64	6.45
21	7.66	7.95		
22	9.08	9.05	9.31	9.24
23	9.36	9.13	9.07	9.18
24	7.23	6.74	7.00	7.15
25	8.90	9.19	9.54	9.35
26	6.18	6.65	7.48	7.37
27	9.15	9.10	8.99	9.33
28	6.72	6.61	7.20	7.38
29	7.66	7.82	7.08	6.78
30	8.66	8.55	8.48	8.26

charge.[21,67] The steric and electrostatic fields are calculated using Lennard−Jones and Coulomb's potentials, respectively. Because functional forms are hyperbolic, both potentials give very large, nonsensical values at or beyond the van der Waals surface. To avoid these values, steric and electrostatic contributions were truncated at 30 kcal/mol (arbitrarily fixed cutoff). In CoMSIA, similarity indices are calculated instead of interaction energies. The functional form in CoMSIA is selected to be Gaussian with an attenuation factor $\alpha = 0.3$. Energy functions typically used to calculate the field values in CoMFA can give rise to significant variation in the energy, with very small changes in position. For example, the Lennard−Jones potential, traditionally used to calculate the steric field, becomes very steep close to the van der Waals surface of the molecule and it may show a singularity at the atomic positions (as does the Coulomb potential used to calculate the electrostatic field). In CoMFA, these issues are dealt with by applying arbitrary cutoffs; the resulting contour plots are thus fragmented and difficult to interpret. In CoMSIA, these fields are replaced by similarity values at the various grid positions. The similarities are calculated using much smoother potentials that are not as steep as the Lennard−Jones and Coulombic functions and have a finite value even at the atomic positions. The use of these similarity indices is considered to lead to superior contour maps that are much easier to interpret.[67]

When correlations are sought using reported data, one must take into account (i) large variability in testing procedures and (ii) uncertainties related to enantiomeric purities of synthetic molecules. A careful examination of published data[7,33,34] identifies essential molecular fragments contributing to "cannabimimetic activity". One of them is the aliphatic C3-side chain; the role of this pharmacophore is important for hydrophobic interactions with the site(s) of action. There is an established SAR that indicates longer side chains are correlated with more potent CBs.[33,68] Decreasing the length of the *n*-pentyl side chain of Δ^9-THC by two carbons reduces potency by 75%.[32] Extension of the five carbon atom chain by adding one or two carbons favors binding, while further extension is detrimental. Interestingly, analogues with substituents, for example, CH_3, C_2H_5, Cl, or I in the ortho position to the phenolic hydroxyl, retain substantial biological activity, however, the para substitution produces inactive analogues.[33,68] Accordingly, para substituents prevent the side chain from orienting to a southern direction with respect to the phenolic hydroxyl group, resulting in decreased CB activity. On the other hand, ortho substitution allows such an orientation.[33] Thus, the orientation of the alkyl side chain plays an important role in the determination of biological activity. A significant degree of conformational restriction can be imposed upon the alkyl side chain either by the introduction of a double bond or by the introduction of a new cyclic ring fused to the aromatic ring A, leading to variations in biological responses.[15] Khanolkar et al.[69] presented a series of Δ^8-THC analogues in which the *n*-heptyl side chain was restricted by a C2−C3 cyclohexyl ring and showed that the side chain pointing downward has an 18-fold higher binding affinity for the CB1 receptor and a 3-fold higher binding affinity for the CB2 receptor than the respective analogue in which the side chain orients laterally. This suggests that the CB receptor affinity decreases significantly when the side chain is forced into a lateral orientation and further away from the ring A.[15,69]

The CB1 and CB2 receptors belong to the same receptor family and exhibit a 44% sequence homology, which rises to 68% in the transmembrane domains, an area thought to be involved in ligand recognition.[7] Because of this high degree of homology, it is not surprising that binding affinities for CB1 and CB2 receptors are correlated. Figures 5a,b and 7a,b show the field contributions to the binding affinity among the CBs and provide a visualization of both steric and electrostatic interactions at the receptor site. The result demonstrates the importance of the hydrophobic components of the classical CBs and other CBs with cannabimimetic activity and is consistent with other studies. The CoMSIA results are in agreement with the CoMFA results. The contour maps resulted by applying CoMFA and CoMSIA methodologies demonstrate that there are similar and different structural requirements for optimum ligand binding at the CB1 and CB2 receptors.

Derived 3D contour maps of CoMFA and CoMSIA models are investigated in the following three distinct regions.

Alkyl Side Chain−Molecular Segment I: The green-colored contours along the left side of the end of the alkyl chain show that bulky groups enhance the binding affinity for the CB1 and CB2 receptors in both CoMFA and CoMSIA models (Figures 5a,b and 7a,b). For example, the presence of adamantane, phenyl, *t*-butyl, isopropyl, or cyclopentyl groups in this region is expected to enhance CB1 and CB2 receptor binding affinities.

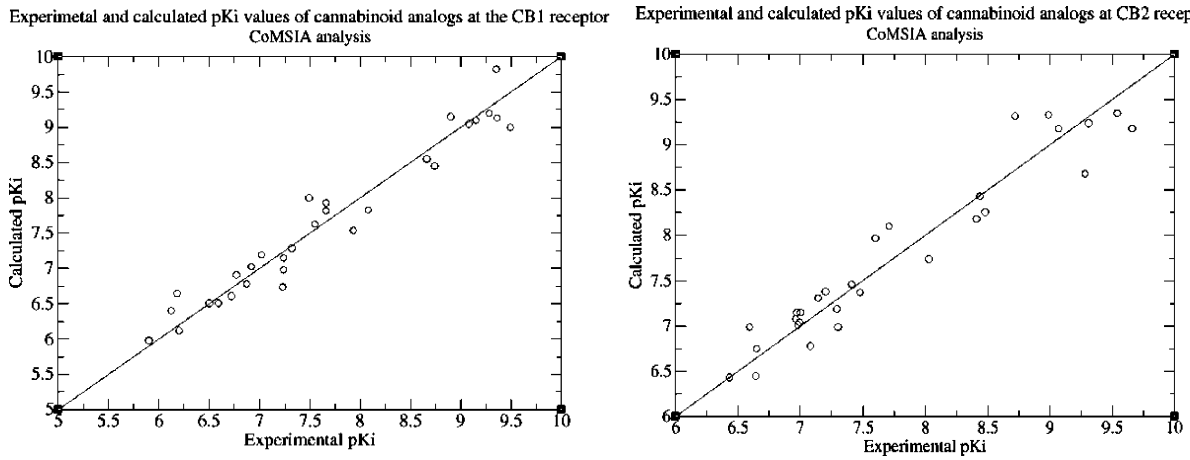

Figure 6. Plots of corresponding CoMSIA-predicted and experimental values of binding affinity (given as pK_i) of CB analogues in the training set at the CB1 (on the left) and CB2 (on the right) receptors, respectively.

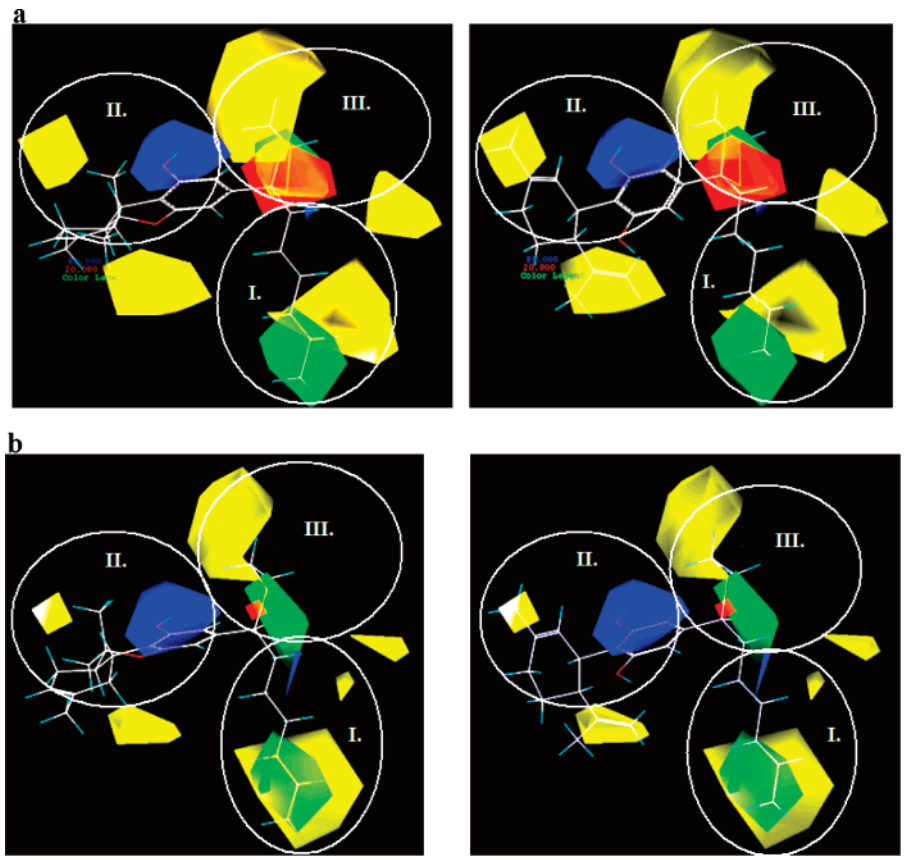

Figure 7. (a) CoMSIA contour maps of template compound **12** (on the left) and its respective CBD analogue **13** (on the right) for the CB1 model. Sterically favored areas are shown in green (contribution level of 80%). Sterically unfavored areas are shown in yellow (contribution level of 20%). Positive potential favored areas are shown in blue (contribution level of 80%). Positive potential unfavored areas are shown in red (contribution level of 20%). (Regions I, II, and III show contour maps around the alkyl side chain, the tricyclic part, and the α-face of C1′ of the ligand, respectively). (b) CoMSIA contour maps of template compound **12** (on the left) and its respective CBD analogue **13** (on the right) for the CB2 model. Sterically favored areas are shown in green (contribution level of 80%). Sterically unfavored areas are shown in yellow (contribution level of 20%). Positive potential favored areas are shown in blue (contribution level of 80%). Positive potential unfavored areas are shown in red (contribution level of 20%). (Regions I, II, and III show contour maps around the alkyl side chain, the tricyclic part, and the α-face of C1′ of the ligand, respectively).

There are large yellow-colored contours on the right side of the end of the alkyl side chain in the CB1 and CB2 CoMSIA models (Figure 7a,b) and small areas for the corresponding CB1 and CB2 CoMFA models (Figure 5a,b) showing the existence of sterically unfavorable fields (the areas in which steric bulk is predicted to decrease binding). Thus, the orientation of the alkyl side chain plays an important role in determining biological activity. This result confirms the previous published reports.[33,56]

Compounds **12**, **14**, **16**, **18**, **22**, **23**, **25**, and **27** show high activity but low selectivity for the CB1 and CB2 receptors attributed to their fit in the hydrophobic subsite of both receptors.[17] An optimal interaction is observed when a lipophilic group is attached to C1′ position. The CB1 receptor

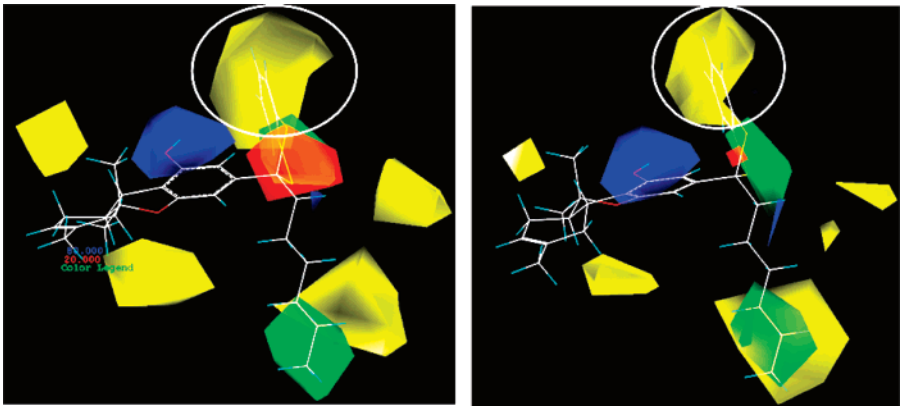

Figure 8. CoMSIA contour maps of **15** for the CB1 (on the left) and the CB2 models (on the right). Sterically favored areas are shown in green (contribution level of 80%). Sterically unfavored areas are shown in yellow (contribution level of 20%). Positive potential favored areas are shown in blue (contribution level of 80%). Positive potential unfavored areas are shown in red (contribution level of 20%).

appears insensitive to isosteric groups attached to the C1′ position whereas the CB2 receptor shows a higher preference for the smaller dioxolane five-membered ring rather than the dithiolane ring or more hydrophobic cyclopentyl analogues.[15]

ABC Ring-Molecular Segment II: The yellow-colored contour at the α-face of the C-ring in the Δ^8-THC analogues (Figures 5a,b and 7a,b, on the left) indicates areas in which steric bulk is predicted to decrease binding. However, in the case of CBD analogues, this area fits on the C9-methyl group (Figures 5a,b and 7a,b, on the right). Bulky groups localized between molecular segments I and II are expected to reduce the binding affinities of CB analogues to both CB1 and CB2 receptors. In these regions, the steric interactions differently affect the binding affinities of Δ^8-THC and CBD analogues for the CB1 and CB2 receptors in both the CoMFA and the CoMSIA models. In Δ^8-THC analogues, a sterically unfavorable area (yellow-colored contour) is located between the regions I and II (Figures 5a,b and 7a,b, on the left). In the case of CBD analogues, because of the different structural orientation of the bicyclic segment, this area fits on the methyl and propenyl groups (Figures 5a,b and 7a,b, on the right). If the binding affinity value of Δ^8-THC analogues and their respective CBD analogues is compared, CBD analogues generally have lower binding affinities than their corresponding Δ^8-THC analogues. For example, the template compound **12**, has 425-fold and 97-fold higher binding affinities than its respective CBD analogue **13**, for CB1 and CB2 receptors, respectively. This can be explained by different topographical requirements for the Δ^8-THC and CBD derivatives at the cyclic ring segment. The CB1 receptor is more sensitive than the CB2 receptor to this different structural orientation, because in this region, the sterically unfavorable area (yellow-colored contour) is larger at the CB1 model (Figures 5a,b and 7a,b).

α-Face of C1′-Molecular Segment III: Sterically unfavorable contour (yellow-colored) is localized in the vicinity of ring A (Figures 5a,b and 7a,b). Therefore, the existence of bulky groups in this molecular segment results in the decrease of the binding affinity as it is confirmed by compounds **15** and **16**. Figure 8 shows the steric-electrostatic CoMSIA contour maps of compound **15** for CB1 and CB2 receptors, respectively. The contour maps show that the increased binding affinity and pharmacological potency are associated with bulky (green-colored contours) and negatively charged groups (red-colored contours) in the α-face of C1′ (Figures 5a,b and 7a,b). The presence of groups such as I^-, C_6H_5OH, $C_6H_5CF_3$, $C_6H_5CCl_3$, $C_6H_5CI_3$, $C_6H_5NH_2$, C_6H_5I, and so on in this region are expected to enhance CB1 and CB2 receptor binding affinities.

The electrostatic contour maps that were correlated with the predicted potency were seen in the α-face of C1′ (molecular segment III) for both of the CoMFA and CoMSIA models and in the middle of the alkyl side chain (molecular segment I) predominantly in the CoMFA models. Results show that in the α-face of C1′ and in the middle of the alkyl side chain, ligands may interact with corresponding electropositive and electronegative atoms of CB1 and CB2 receptors, respectively (Figures 5a,b and 7a,b).

To test the stability of the obtained PLS models for every conventional CoMFA and CoMSIA PLS run, bootstrapping was also performed. Obtained results support the reliability of the created models.

In addition, to test the predictive ability of the obtained CoMFA and CoMSIA models, 20 other Δ^8-THC analogues have been added to the training set for the CB1 model and 12 other Δ^8-THC analogues have been added to the training set for the CB2 model. (Binding affinities have been taken from reported values in the literature.[15,17] Binding affinities of eight CB analogues have been measured only for the CB1 receptor.) The same CoMFA and CoMSIA settings and PLS analyses have been performed for the reconstructed CoMFA and CoMSIA models. Compound **12** has been used as a template and the same atoms in the CoMFA and CoMSIA models have been selected for the structural superimposition processes for reconstructed models. The results did not significantly modify the initially obtained models. The reconstructed 3D-QSAR CoMFA and CoMSIA models for the binding affinities to the CB1 and CB2 receptors have a very good cross-validated correlation. Although there are minor differences between initial and reconstructed CoMFA and CoMSIA models, the overall emerging picture is consistent. The main topographical requirements in the reconstructed CoMFA and CoMSIA models confirm the initially obtained models for the CB1 and CB2 receptors. The predictive ability of the initial model has been tested with added compounds and it was shown that the model is able to accurately predict them as true unknowns. (This part is included in the Supporting Information.)

Summary and Conclusions

In summary, the present research work describes a successful attempt to conduct a molecular modeling and NMR-based 3D-QSAR CoMFA and CoMSIA studies of the CB1 and CB2 agonist pharmacophore models.

The CoMFA and CoMSIA models provided similar results, however, the steric interactions in CoMSIA models are more dominant. It is evident from the contour maps of CB1 and CB2 models of CoMFA and CoMSIA that the steric effects determine the binding affinity. The relative contributions of steric fields are larger than electrostatic fields for both CB1 and CB2 models in both of the CoMFA and CoMSIA analyses. The orientation of the C3-alkyl side chain plays a crucial role in determining the biological activity; bulky groups at the end of the left sides of C3-alkyl side chain (corresponding to shown snapshot contour plots) of compounds lead to enhancement of the activity, whereas bulky groups in the right sides of the C3-alkyl side chain of analogues lead to decreased binding affinity.

Because of the different structural properties of Δ^8-THC and CBD derivatives at the cyclic ring segment, these groups have different pharmacophoric requirements for their receptors in these regions. While sterically unfavorable areas are located on the methyl and propenyl groups of CBD analogues, these unfavorable regions are located at the vicinity of the tricyclic segment of Δ^8-THC analogues. Therefore, Δ^8-THC analogues have higher binding affinities than their respective CBD analogues. The partial positive charge in the C1′−C3′ region of the alkyl side chain and the partial negative charge occupied in the α-face of C1′ are predicted to interact productively within the corresponding site(s) of the receptors.

The obtained models will serve as a basis for the design of novel CB-like prototypes with enhanced activity and other tailored properties. The information on the receptor binding sites also provides an opportunity for the design of specific probes to be used in studies seeking to elucidate the mechanism of action of these drug molecules.

Computational Methods

(i) Binding Affinities. The binding affinities (K_i) were assessed by a quantitative assay based on the affinity of CB analogues to CB1 and CB2 receptors. The logarithmic values of $1/K_i$ (pK_i) were used in the 3D-QSAR correlations, as they are related to changes in the free energy of binding. Table 1 lists all the structures used in the training set and their experimental binding affinities (K_i) at CB1 and CB2 receptors.[34,56−59]

(ii) Molecular Modeling. The structures of the studied molecules were subjected to full geometry optimization using a combination of the standard Tripos molecular mechanic force field of the Sybyl molecular modeling package[70] (Powel energy minimization algorithm,[71] Gasteiger−Huckel charges,[72] and 0.001 kcal/mol Å energy gradient convergence criterion), Monte Carlo analysis with the CHARMm force field of QUANTA package[73] (Powel energy minimization algorithm, Gasteiger−Huckel charges, and 0.001 kcal/mol Å energy gradient convergence criterion) as well as the semiempirical methods of AM1[74] and PM3[75] methods (SCF convergence criterion has been set to 10^{-6} as energy gradient convergence limit). For the conformational analysis of template compound **12** ab initio B3LYP/6-31G*[65,66] level quantum mechanics calculations were also performed.

(iii) CoMFA Settings. CoMFA was performed using the QSAR option of Sybyl. The steric and electrostatic field energies were calculated using the Lennard−Jones and the Coulomb potentials, respectively, with a $1/r$ distance-dependent dielectric constant in all intersections of a regularly spaced (0.2 nm) grid.[67] A sp^3 carbon atom with a radius of 1.53 Å and a charge of +1.0 was used as a probe to calculate the steric and electrostatic energies between the probe and the molecules using the Tripos force field.[76] The truncation for both the steric and the electrostatic energies were set to 30 kcal/mol. This indicates that any steric or electrostatic field value that exceeds this value will be replaced with 30 kcal/mol, thus makes a plateau of the fields close to the center of any atom.

(iv) CoMSIA Settings. CoMSIA was performed using the QSAR option of Sybyl. A sp^3 carbon atom with a radius of 1.53 Å and a charge of +1.0 was used as the probe to calculate the CoMSIA similarity indices. Steric and electrostatic similarity indices were evaluated at the intersections of a similar grid using the same probe atom according to the standard implementation of CoMFA in Sybyl. The similarity indices between the compounds and the probe atom are calculated according to

$$A_{F,k}^{q}(j) = -\sum_{i=1}^{n} w_{probe,k} w_{ik} e^{-\alpha r_{iq}^2}$$

where A is the similarity index at the grid point q, summed over all atoms i of the molecule j under investigation; $w_{probe,k}$ is the probe atom; w_{ik} is the actual value of the physicochemical property k of atom i; r_{iq} is the mutual distance between the probe atom at grid point q and atom i of the test molecule; and α is the attenuation factor.[47]

The default value of attenuation factor α was set to 0.3. Larger values of α will result in a steeper Gaussian function and increasing attenuation of the distance-dependent effects of molecular similarity. On the other hand, reducing α to smaller values will result in a probe atom detecting molecular similarity of its neighborhood more globally. The optimal value of α is between 0.2 and 0.4.[77]

(v) CoMFA and CoMSIA Partial Least-Squares (PLS) Analysis and Validations. The initial PLS analysis was performed using the "leave-one-out" cross-validation method for all 3D-QSAR analyses. A minimum column filtering value of 2.00 kcal/mol was set to improve the signal-to-noise ratio by omitting those grid points whose energy variation was below this threshold. In both CoMFA and CoMSIA analyses, descriptors were treated as independent variables, whereas the pK_i values were treated as dependent variables in the PLS regression analyses to derive the 3D-QSAR models. The final model (noncross-validated conventional analysis) was developed from the model with the highest r_{cv}^2, and the optimum number of components was set to equal that yielding the highest r_{cv}^2. The noncross-validated models were assessed by the conventional correlation coefficient r^2, standard error of prediction, and F values. For the creation of the CoMFA field, "CoMFA standard" scaling was selected, while in the case of CoMSIA, the "none" option was selected in the Sybyl.

To obtain confidence limits and test the stability of obtained PLS models, for every conventional CoMFA and CoMSIA PLS run, bootstrapping was also performed (100 runs, column filtering: 2.00 kcal/mol). The idea is to simulate a statistical sampling procedure by assuming that the original data set is the true population and generating many new data sets from it. These new data sets (called bootstrap samplings) are of the same size as the original data set and are obtained by randomly choosing samples (rows) from the original data, with repeated selection of the same row being allowed. The statistical calculation is performed on each of these bootstrap samplings, with new values being calculated for each of the parameters to be estimated. The difference between the parameters calculated from the original data set and the average of the parameters calculated from the many bootstrap samplings is a measure of the bias of the original calculation.[78]

The "quality" of a simple or multiple linear regression can be assessed in a number of ways. The most common of these is to calculate the *squared correlation coefficient*, r^2 value. This has a value between zero and one and indicates the proportion of the variation in the dependent variable that is explained by the regression equation. Suppose $y_{calc,i}$ are the values obtained by feeding the relevant independent variables into the regression equation and y_i are the corresponding measured observations. The following quantities can then be calculated[67]

$$\text{total sum of squares (TSS)} = \sum_{i=1}^{N} (y_i - \langle y \rangle)^2$$

$$\text{explained sum of squares (ESS)} = \sum_{i=1}^{N}(y_{\text{calc},i} - \langle y \rangle)^2$$

$$\text{residual sum of squares (RSS)} = \sum_{i=1}^{N}(y_i - y_{\text{calc},i})^2$$

Thus, TSS = ESS + RSS and r^2 is given by the following equation

$$r^2 = \text{ESS/TSS} \equiv 1 - (\text{RSS/TSS})$$

Cross-validated PLS analysis was run to determine the optimal number of components in the model and to evaluate the robustness of the model based on quality of predictability. Cross-validation methods provide a way to try and overcome some of the problems inherent in the use of the r^2 value alone. Cross-validation involves the removal of some of the values from the training set, the derivation of a QSAR model using the remaining data, and then the application of this model to predict the values of the data that have been removed. One form of cross-validation method is the *leave one out* approach, where only one data value is removed from data set. Repeating this procedure for every value in the data set leads to a r^2_{cv}. To build a 3D-QSAR model for the CB ligand/CB receptor complex, the PLS analysis was repeated until the biological property value has been "predicted" by a model from where these were derived. There is a generally accepted criterion for statistical validity of $r^2_{cv} \geq 0.6$.[48]

Acknowledgment. This work is financially supported by the European Union within the 6th Framework Programme-Marie Curie Actions. (Project: EURODESY-MEST-CT-2005-020575). We would like to thank Kyra-Melinda Alexacou and Robert Feldman for their technical assistance.

Supporting Information Available: Tables that summarize the topographical requirements for CB1 and CB2 receptors using CoMFA and CoMSIA approaches. Molecular structures and binding affinity values of Δ^8-THC analogues for the reconstructed CoMFA and CoMSIA models, structural superimposition of analogues, results of cross-validated and noncross-validated analyses at the CB1 and CB2 receptors using the reconstructed CoMFA and CoMSIA models, plots of corresponding reconstructed CoMFA and CoMSIA calculated and experimental values of binding affinity of CB analogues in the training set at the CB1 and CB2 receptors, and CoMFA/CoMSIA contour maps of template compound **12** and its respective CBD analogue **13** for the reconstructed CB1 and CB2 models. This material is available free of charge via the Internet at http://pubs.acs.org.

References

(1) Gaoni, Y.; Mechoulam, R. Isolation, structure and partial synthesis of an active constituent of hashish. *J. Am. Chem. Soc.* **1964**, *86*, 1646−1647.
(2) Devane, W. A.; Dysarz, F. A.; Johnson, M. R.; Melvin, L. S.; Howlett, A. C. Determination and characterization of a cannabinoid receptor in rat brain. *Mol. Pharmacol.* **1988**, *34*, 605−613.
(3) Gerard, C. M.; Mollereau, C.; Parmentier, M. Nucleotide sequence of a human cannabinoid receptor cDNA. *Nucleic Acid Res.* **1990**, *18*, 7142−7148.
(4) Matsuda, L. A.; Lolait, S. J.; Brownstein, M. J.; Young, A. C.; Bonner, T. I. Structure of a cannabinoid receptor and functional expression of the cloned cDNA. *Nature* **1990**, *346*, 561−564.
(5) Gerard, C. M.; Mollereau, C.; Vassart, G.; Parmentier, M. Molecular cloning of a human cannabinoid receptor which is also expressed in testis. *Biochem. J.* **1991**, *279*, 129−134.
(6) Munro, S.; Thomas, K. L.; Abu-Shar, M. Molecular characterization of a peripheral receptor for cannabinoids. *Nature* **1993**, *365*, 61−65.
(7) Reggio, P. H. Pharmacophores for ligand recognition and activation/inactivation of the cannabinoid receptors. *Curr. Pharm. Des.* **2003**, *9*, 1607−1633.
(8) Padgett, L. W. Recent developments in cannabinoid ligands. *Life Sci.* **2005**, *77*, 1767−1798.
(9) Sugiura, T.; Kishimoto, S.; Oka, S.; Gokoh, M. Biochemistry, pharmacology and physiology of 2-arachidonoylglycerol, an endogenous cannabinoid receptor ligand. *Prog. Lipid Res.* **2006**, *45*, 405−446.
(10) Herkenham, M.; Lynn, A. B.; Little, M. D.; Johnson, M. R.; Melvin, L. S.; De Costa, B. R.; Rice, K. C. Cannabinoid receptor localization in brain. *Proc. Natl. Acad. Sci. U.S.A.* **1990**, *87*, 1932−1936.
(11) Glass, M.; Dragunow, M.; Faull, R. L. Cannabinoid receptors in the human brain: a detailed anatomical and quantitative autoradiographic study in the fetal, neonatal and adult human brain. *Neuroscience* **1997**, *77* (2), 299−318.
(12) Straiker, A. J.; Maguire, G.; Makie, K.; Lindsey, J. Localization of cannabinoid CB1 receptors in the human anterior eye and retina. *Invest. Ophthalmol. Visual. Sci.* **1999**, *40*, 2442−2448.
(13) Pertwee, R. G.; Fernando, S. R. Evidence for the presence of cannabinoid CB1 receptors in mouse urinary bladder. *Br. J. Pharmacol.* **1996**, *118*, 2053−2058.
(14) Klein, T. W.; Newton, C.; Friedman, H. Cannabinoid receptors and immunity. *Immunol. Today* **1998**, *19*, 373−381.
(15) Thakur, G. A.; Duclos, R. I., Jr.; Makriyannis, A. Natural cannabinoids: Templates for drug discovery. *Life Sci.* **2005**, *78*, 454−466.
(16) Fichera, M.; Cruciani, G.; Bianchi, A.; Musumarra, G. A 3D-QSAR study on the structural requirements for binding to CB(1) and CB(2) cannabinoid receptors. *J. Med. Chem.* **2000**, *43*, 2300−2309.
(17) Khanolkar, A. D.; Palmer, S. L.; Makriyannis, A. Molecular probes for the cannabinoid receptors. *Chem. Phys. Lipids* **2000**, *108*, 37−52.
(18) Galie'gue, S.; Mary, S.; Marchand, J.; Dussossoy, D.; Carriere, D.; Carayon, P.; Bouaboula, M.; Shire, D.; Le Fur, G.; Casellas, P. Expression of central and peripheral cannabinoid receptors in human immune tissues and leukocyte subpopulations. *Eur. J. Biochem.* **1995**, *232*, 54−61.
(19) Oz, M. Receptor-independent actions of cannabinoids on cell membranes: Focus on endocannabinoids. *Pharmacol. Ther.* **2006**, *111*, 114−144.
(20) Parkkari, T.; Savinainen, J. R.; Raitio, K. H.; Saario, S. M.; Matilainen, L.; Sirvio, T.; Laitinen, J. T.; Nevalainen, T.; Niemi, R.; Jarvinen, T. Synthesis, cannabinoid receptor activity, and enzymatic stability of reversed amide derivatives of arachidonoyl ethanolamide. *Bioorg. Med. Chem.* **2006**, *14*, 5252−5258.
(21) Salo, O. M. H.; Savinainen, J. R.; Parkkari, T.; Nevalainen, T.; Lahtela-Kakkonen, M.; Gynther, M.; Laitinen, J. T.; Jarvinen, T.; Poso, A. 3D-QSAR studies on cannabinoid CB1 receptor agonists: G-protein activation as biological data. *J. Med. Chem.* **2006**, *49*, 554−566.
(22) Lambert, D. M.; Fowler, C. J. The endocannabinoid system: Drug targets, lead compounds, and potential therapeutic applications. *J. Med. Chem.* **2005**, *48* (16), 1−29.
(23) Felder, C. C. Endocannabinoids and their receptors as targets for treating metabolic and psychiatric disorders. *Drug Discovery Today* **2006**, *3* (4), 561−567.
(24) Devane, W. A.; Hanus, L.; Breuer, A.; Pertwee, R. G.; Stevenson, L. A.; Griffin, G.; Gibson, D.; Mandelbaum, A.; Etinger, A.; Mechoulam, R. Isolation and structure of a brain constituent that binds to the cannabinoid receptor. *Science* **1992**, *258*, 1946−1949.
(25) Lin, S.; Khanolkar, A. D.; Fan, P.; Goutopoulos, A.; Qin, C.; Papahadjis, D.; Makriyannis, A. Novel analogues of arachidonylethanolamide (anandamide); affinities for the CB1 and CB2 cannabinoid receptors and metabolic stability. *J. Med. Chem.* **1998**, *41*, 5353−5361.
(26) Sugiura, T.; Kondo, S.; Sukugawa, A.; Nakane, S.; Shinoda, A.; Itoh, K.; Yamashita, A.; Waku, K. 2-Arachidonoylglycerol: A possible endogenous cannabinoid receptor ligand in brain. *Biochem. Biophys. Res. Commun.* **1995**, *215*, 89−97.
(27) Mechoulam, R.; Ben-Shabat, S.; Hanus, L.; Ligumsky, M.; Kaminski, N. E.; Schatz, A. R.; Gopher, A.; Almog, S.; Martin, B. R.; Compton, D. R.; Pertwee, R. G.; Griffin, G.; Bayewitch, M.; Barg, J.; Vogel, Z. Identification of an endogenous 2-monoglyceride, present in canine gut, that binds to cannabinoid receptors. *Biochem. Pharmacol.* **1995**, *50*, 83−90.
(28) Stella, N.; Schweitzer, P.; Piomelli, D. A second endogenous cannabinoid that modulates long-term potentiation. *Nature* **1997**, *388*, 773−778.
(29) Mackie, K. Cannabinoid receptors as therapeutic targets. *Annu. Rev. Pharmacol. Toxicol.* **2006**, *46*, 101−122.
(30) Felder, C. C.; Glass, M. Cannabinoid receptors and their endogenous agonists. *Annu. Rev. Pharmacol. Toxicol.* **1998**, *38*, 179−200.
(31) Palmer, S. L.; Thakur, G. A.; Makriyannis, A. Cannabinergic ligands. *Chem. Phys. Lipids* **2002**, *121*, 3−19.
(32) Razdan, R. K. Structure-activity relationships in cannabinoids. *Pharmacol. Rev.* **1986**, *38*, 75−149.
(33) Makriyannis, A.; Rapaka, R. S. The molecular basis of cannabinoid activity. *Life Sci.* **1990**, *47*, 2173−2184.

(34) Papahatjis, D. P.; Kourouli, T.; Abadji, V.; Goutopoulos, A.; Makriyannis, A. Pharmacaphoric requirements for the cannabinoid side chains: Multiple bond and C1′-substituted Δ^8-tetrahydrocannabinols. *J. Med. Chem.* **1998**, *41*, 1195−1200.
(35) Xie, X-Q.; Pavlopoulos, S.; DiMeglio, C. M.; Makriyannis, A. Conformational studies on a diastereoisomeric pair of tricyclic nonclassical cannabinoids by NMR spectroscopy and computer molecular modeling. *J. Med. Chem.* **1998**, *41* (2), 167−174.
(36) Melvin, L. S.; Johnson, M. R. Structure-activity relationships of tricyclic and non- classical bicyclic cannabinoids. *NIDA Res. Monogr.* **1987**, *79*, 31−47.
(37) Howlett, A. C.; Johnson, M. R.; Melvin, L. S.; Milne, G. M. Nonclassical cannabinoid analgetics inhibit adenylate cyclase: Development of a cannabinoid receptor model. *Mol. Pharmacol.* **1988**, *33* (3), 297−302.
(38) Mavromoustakos, T.; Theodoropoulou, E.; Zervou, M.; Kourouli, T.; Papahatjis, D. Structure elucidation and conformational properties of synthetic cannabinoids (−)-2-(6a,7,10,10a-tetrahydro-6,6,9-trimethyl-1-hydroxy-6*H*-dibenzo[b,d]pyranyl)-2-hexyl-1,3-dithiolane and its methylated analog. *J. Pharm. Biomed. Anal.* **1999**, *18*, 947−956.
(39) Keimowitz, A. R.; Martin, B. R.; Razdan, R. K.; Crocker, P. J.; Mascarella, S. W.; Thomas, B. F. QSAR analysis of Δ^8-THC analogues: Relationship of side-chain conformation to cannabinoid receptor affinity and pharmacological potency. *J. Med. Chem.* **2000**, *43*, 59−70.
(40) Shire, D.; Calandra, B.; Delpech, M.; Dumont, X.; Kaghad, M.; Le Fur, G.; Caput, D.; Ferrara, P. Structural features of the central cannabinoid CB1 receptor involved in the binding of the specific CB1 antagonist SR 141716A. *J. Biol. Chem.* **1996**, *271*, 6941−6946.
(41) Reggio, P. H.; Panu, A. M.; Miles, S. Characterization of a region of steric interference at the cannabinoid receptor using the active analogue approach. *J. Med. Chem.* **1993**, *36*, 1761−1771.
(42) Semus, S. F.; Martin, B. R. A computer graphic investigation into the pharmacological role of the THC-cannabinoid phenolic moiety. *Life Sci.* **1990**, *46*, 1781−1785.
(43) Shim, J. Y.; Collantes, E. R.; Welsh, W. J.; Subramaniam, B.; Howlett, A. C.; Eissenstat, M. A.; Ward, S. J. Three-dimensional quantitative structure-activity relationship study of the cannabimimetic (aminoalkyl)indoles using comparative molecular field analysis. *J. Med. Chem.* **1998**, *41*, 4521−4532.
(44) Thomas, B. F.; Compton, D. R.; Martin, B. R.; Semus, S. F. Modeling the cannabinoid receptor: a three-dimensional quantitative structure-activity analysis. *Mol. Pharmacol.* **1991**, *40*, 656−665.
(45) Thomas, B. F.; Adams, I. B.; Mascarella, S. W.; Martin, B. R.; Razdan, R. K. Structure activity analysis of anandamide analogues: relationship to a cannabinoid pharmacophore. *J. Med. Chem.* **1996**, *39*, 471−479.
(46) Cramer, R. D. I.; Depriest, S.; Patterson, D.; Hecht, P. In *The developing practice of comparative molecular field analysis*; Kubinyi, H., Ed.; ESCOM: Leiden, 1993; pp 443−485.
(47) Klebe, G.; Abraham, U.; Mietzner, T. Molecular similarity indices in a comparative analysis (CoMSIA) of drug molecules to correlate and predict their biological activity. *J. Med. Chem.* **1994**, *37*, 4130−4146.
(48) Chen, J-Z.; Han, X-W.; Liu, Q.; Makriyannis, A.; Wang, J.; Xie, X-Q. 3D-QSAR studies of arylpyrazole antagonists of cannabinoid receptor subtypes CB1 and CB2. A combined NMR and CoMFA approach. *J. Med. Chem.* **2006**, *49*, 625−636.
(49) Doytchinova, I. A.; Flower, D. R. Towards the quantitative prediction of T-cell epitopes: CoMFA and CoMSIA studies of peptides with affinity to class I MHC molecule HLA-A*0201. *J. Med. Chem.* **2001**, *44*, 3572−3581.
(50) Folkers, G.; Merz, A.; Rognan D. CoMFA: Scope and Limitations. In *3D QSAR in Drug Design*; Kubinyi, H., Ed.; ESCOM: Leiden, 1993; pp 583−618.
(51) Tong, W.; Collantes, E. R.; Welsh, W. J.; Berglund, B. A.; Howlett, A. C. Derivation of a pharmacophore model for anandamide using constrained conformational searching and comparative molecular field analysis. *J. Med. Chem.* **1998**, *41*, 4207−4215.
(52) Kapou, A.; Benetis, N. P; Avlonitis, N.; Calogeropoulou, T., Koufaki, M.; Scoulica, E., Nikolaropoulos, S. S.; Mavromoustakos, T. 3D-Quantitative structure−activity relationships of synthetic antileishmanial ring-substituted ether phospholipids. *Bioorg. Med. Chem.* **2007**, *15*, 1252−1265.
(53) Schmetzer, S.; Greenidge, P.; Kovar, K. A.; Schulze-Alexandru, M.; Folkers, G. Structure-activity relationships of cannabinoids: A joint CoMFA and pseudoreceptor modelling study. *J. Comput.-Aided Mol. Des.* **1997**, *11*, 278−292.
(54) Xie, A.; Sivaprakasam, P.; Doerksen, R. J. 3D-QSAR analysis of antimalarial farnesyltransferase inhibitors based on a 2,5-diaminobenzophenone scaffold. *Bioorg. Med. Chem.* **2006**, *14*, 7311−7323.
(55) Cramer, R. D., III; Patterson, D. E.; Bunce, J. D. Comparative molecular field analysis (CoMFA) 1. Effect of shape on binding of steroids to carrier proteins. *J. Am. Chem. Soc.* **1988**, *110*, 5959−5967.
(56) Papahatjis, D. P.; Nikas, S. P.; Kourouli, T.; Chari, R.; Xu, W.; Pertwee, R. G.; Makriyannis, A. Pharmacophoric requirements for the cannabinoid side chain. Probing the cannabinoid receptor subsite at C1′. *J. Med. Chem.* **2003**, *46*, 3221−3229.
(57) Papahatjis, D. P.; Nahmias, V. R.; Andreou, T.; Fan, P.; Makriyannis, A. Structural modifications of the cannabinoid side chain towards C3-aryl and 1′,1′-cycloalkyl-1′-cyano cannabinoids. *Bioorg. Med. Chem. Lett.* **2006**, *16*, 1616−1620.
(58) Papahatjis, D. P.; Nikas, S. P.; Andreou, T.; Makriyannis, A. Novel 1′,1′-chain-substituted Δ^8-tetrahydrocannabinols. *Bioorg. Med. Chem. Lett.* **2002**, *12*, 3583−3586.
(59) Gareau, Y.; Dufrense, C.; Gallant, M.; Rochette, C.; Sawyer, N.; Slipetz, D. M.; Tremblay, N.; Weech, P. K.; Metters, K. M.; Labelle, M. Structure−activity relationships of tetrahydrocannabinol analogues on human cannabinoid receptor. *Bioorg. Med. Chem. Lett.* **1996**, *6*, 189−194.
(60) Xie, X.-Q.; Yang, D.-P.; Melvin, L. S.; Makriyannis, A. Conformational analysis of the prototype nonclassical cannabinoid CP-47,-497, using 2D NMR, and computer molecular modeling. *J. Med. Chem.* **1994**, *37*, 1418−1426.
(61) Xie, X-Q.; Melvin, L. S.; Makriyannis, A. The conformational properties of the highly selective cannabinoid receptor ligand CP-55,940. *J. Biol. Chem.* **1996**, *71*, 169−189.
(62) Shim, J-Y.; Welsh, W. J.; Howlett, A. C. Homology model of the CB1 cannabinoid receptor: Sites critical for nonclassical cannabinoid agonist interaction. *Biopolymers* **2003**, *71*, 169−189.
(63) Makriyannis, A. In *Cannabinoid Receptors; Chapter 3: The role of cell membranes in cannabinoid activity*; Pertwee, R., Ed.; Academic Press Limited: London, 1995; pp 87−115.
(64) Mavromoustakos, T.; Zervou, M.; Zoumpoulakis, P.; Kyrikou, I.; Benetis, N. P.; Polevaya, L.; Roumelioti, P.; Giatas, N.; Zoga, A.; Moutevelis Minakakis, P.; Kolocouris, A.; Vlahakos, D.; Golic Grdadolnik, S.; Matsoukas, J. Conformation and bioactivity, design and discovery of novel antihypertensive drugs. *Curr. Top. Med. Chem.* **2004**, *4*, 385−401.
(65) Becke, A. D. Density-functional thermochemistry III. The role of exact exchange. *J. Chem. Phys.* **1993**, *98*, 5648−5662.
(66) Hehre, W. J.; Ditchfield, R.; Pople, J. A. Self-consistent molecular orbital methods. XV. Extended Gaussian-type basis sets for lithium, beryllium, and boron. *J. Chem. Phys.* **1975**, *62*, 2921.
(67) Leach, A. R.; Gillet, V. J. *An Introduction to Chemoinformatics*; Kluwer Academic Publishers: Dordrecht, 2003.
(68) Loev, B.; Bender, P. E.; Dawalo, F.; Macko, E.; Fowler, P. J. Cannabinoids. Structur−-activity studies related to 1,2-dimethylheptyl derivatives. *J. Med. Chem.* **1973**, *16*, 1200- 1206.
(69) Khanolkar, A. D.; Lu, D.; Fan, P.; Tian, X.; Makriyannis, A. *Bioorg. Med. Chem. Lett.* **1999**, *9*, 2119.
(70) *Sybyl*, v. 6.8., molecular modeling software packages; Tripos Inc.: St Louis, MO 63144, 2001.
(71) Powell, M. J. D. Restart Procedures for the Conjugate Gradient Method. *Math. Prog.* **1977**, *12*, 241−254.
(72) Gasteiger, J.; Marsili, M. Iterative partial equalization of orbital electronegativity-a rapid access to atomic charges. *Tetrahedron* **1980**, *36*, 3219−3228.
(73) Brooks, B. R.; Bruccoleri, R. E.; Olafson, B. D.; States, D. J.; Swaminathan, S.; Karplus, M. CHARMM: A program for macromolecular energy, minimization, and dynamics calculations. *J. Comp. Chem.* **1983**, *4*, 187−217.
(74) Dewar, M. J. S.; Zoebisch, E. G.; Healy, E. F.; Stewart, J. J. P. Development and use of quantum mechanical molecular models. AM1: A new general purpose quantum mechanical molecular model. *J. Am. Chem. Soc.* **1985**, *107*, 3902−3909.
(75) Stewart, J. J. P. Optimization of parameters for semi-empirical methods I-method. *J. Comp. Chem.* **1989**, *10*, 209−220.
(76) Clark, M.; Cramer, R. D., III.; Van, Opdenbosch, N. Validation of the general purpose Tripos 5.2 force field. *J. Comput. Chem.* **1989**, *10*, 982−1012.
(77) Böhm, M.; Stürzebecher, J.; Klebe, G. 3D QSAR Analyses using CoMFA and CoMSIA to elucidate selectivity differences of inhibitors binding to trypsin, thrombin and factor Xa. *J. Med. Chem.* **1999**, *42*, 458−477.
(78) Tripos Bookshelf, v. 6.8; Tripos Inc.: St Louis, MO 63144, 2001.

JM0610705